

# ACCURATE ENERGY PREDICTIONS FOR TRACKING HCPV INSTALLATIONS

M McDonald\*, J Dittmer  
SolFocus, Inc.

\*510 Logue Ave, Mountain View, CA 94043, USA, jeremy\_dittmer@solfocus.com

**ABSTRACT:** High efficiency high concentration photovoltaic (HCPV) solar plants of megawatt scale are now installed and operational. Wide utility adoption of HCPV requires reliable prediction of energy production for site planning and operation. HCPV module nameplate power is rated for specific test conditions; however, instantaneous HCPV power varies due to site specific irradiance and is impacted, in part, by operating temperature, soiling, protective stowing, solar spectrum, shading, and electrical connectivity. We will show a time sequence model accurately accounting for these effects that predicts annual energy production, and can be used to guide cost-effective site selection, plant layout and operation, and system-level design decisions.

**Keywords:** Concentrated photovoltaics, HCPV, solar energy models

## 1 INTRODUCTION

Photovoltaic (PV) and High Concentration PV (HCPV) solar energy production require an upfront capital investment which is to be recouped from the production and sale of electrical energy over the life of the solar system. The electrical energy harvested varies significantly by site according to time dependent losses from weather and shading among other factors, adding risk to analysis of return on investment and possibly delaying or deterring project development. The PV segment has a history of large-scale deployments with more than 5 years of data that provide background for estimation of electrical energy harvest, at least when assessing new sites with similar characteristics. The HCPV segment has several moderate-scale deployments [1], but with a more limited range of sites and history. An accurate, rapid means of analytically assessing the suitability of sites and site designs for PV and particularly for HCPV can assure the best possible return on the invested capital, and is an enabler of expanding investment in, and grid penetration of, HCPV solar energy.

This need for rapid site design assessment has led to the development of several software tools for PV simulation [2] [3] [4] [5]. An accurate HCPV energy simulation tool must include temperature and spectral-mismatch effects on cell performance, shading arising from horizon as well as other HCPV systems, and an accurate accounting for the electrical interconnections prevalent for HCPV at a fine temporal granularity. While many of the PV codes offer a HCPV mode, they can lack support for the Direct Normal Irradiance (DNI) solar resource, for 2-axis tracking, for necessary electrical string layouts interconnection, or for horizon shading and topography.

Owing to the specific benefits and requirements for accurate simulation of HCPV plants, and the limitations of present PV codes in accurately assessing HCPV, we have created a model that includes relevant environmental, shading, and string effects. We will derive the models used for that simulation tool, and demonstrate results for the estimation of energy harvest at varying sites and scales.

## 2 TIME SEQUENCE ENERGY MODEL

SolFocus' time sequence energy model is the numeric integration of power for all time samples within a target time period. The power is calculated using a form shown in Equation 1.

$$P_{DC,Actual}[t] = P_{DC,Rated}[t] \times \left( \frac{DNI[t]}{DNI_{Rated}} \right) \times S[t] \times F[t] \times O[t]$$

**Equation 1:** Instantaneous power from solar array

Where power produced is normalized to the rated power as well as the rated DNI.  $S[t]$ ,  $F[t]$  and  $O[t]$  represent losses incurred due to shading, environmental factors, and others. Each of these loss categories will be addressed in detail below.

### 2.1 Shading model – self-shading

The most complex shading loss to calculate is caused by shadows cast by other moving arrays. This geometric problem increases in complexity as the square of the number of systems involved since each array might be shaded by any of the other arrays. The algorithm developed by SolFocus captures these shading effects at the level of individual modules to permit accurate electrical analysis. The self-shading algorithm relies on latitude and longitude locations being specified for each separate tracking array.

For practical purposes, a field of arrays tracking the sun will all be in parallel planes. It is useful to do some rotations and translations to the dimensions and latitude/longitude locations of the arrays so that the array apertures all appear as rectangles in X-Y in different Z planes. This is akin to viewing the arrays from the vantage point of the sun. In this coordinate system, shading can be more easily calculated by examining how the rectangles intersect one another. The necessary transformations are described in detail below.

We define a world coordinate system in which an array positioned at the intersection of the equator and prime meridian and oriented towards the northern horizon will have a horizontal centerline coincident with the X-axis, a vertical centerline coincident with the Y-axis and normal vector coincident with the Z-axis (see Figure 1). Each array starts in this location with this orientation. Only the lower left corner (as viewed along a negative Z direction with positive Y up) is tracked through the transformations since the rectangle that

represents the array aperture can be reconstructed using the array's mechanical dimensions. The coordinates of this point in the defined coordinate system are  $[-(array\ width)/2, -(array\ height)/2, 0]$ .

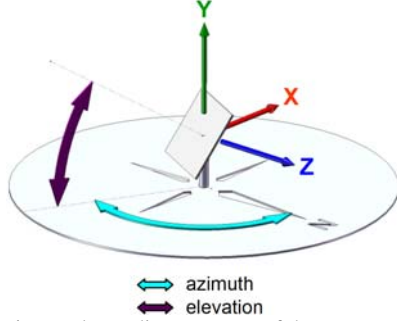


**Figure 1:** Local coordinate system of the array

The ephemeris equations are used to calculate the desired azimuth and elevation for the array's actual position on earth at the time of interest and these are applied to the array by rotating about the X-axis for elevation followed by a rotation about the Y-axis for azimuth. The negative of both elevation and azimuth angles are used so that the rotation direction will be correct in a right-handed coordinate system. These rotations can be represented with the matrix multiplications (see Equation 2) where point  $[X_0, Y_0, Z_0]^T$  is the lower left corner of the array in its originally defined position and  $[X_1, Y_1, Z_1]^T$  represents the point's location following the rotation.

$$\begin{bmatrix} \cos(-az) & 0 & \sin(-az) \\ 0 & 1 & 0 \\ -\sin(-az) & 0 & \cos(-az) \end{bmatrix} \begin{bmatrix} 1 & 0 & 0 \\ 0 & \cos(-el) & -\sin(-el) \\ 0 & \sin(-el) & \cos(-el) \end{bmatrix} \begin{bmatrix} X_0 \\ Y_0 \\ Z_0 \end{bmatrix} = \begin{bmatrix} X_1 \\ Y_1 \\ Z_1 \end{bmatrix}$$

**Equation 2:** Coordinate transformation to ephemeral orientation

The arrays are then translated to reflect the dimensions of earth (see Equation 3). This translation is equivalent to moving the origin of the coordinate system to earth's center while positioning the array at its correct altitude. With this transformation, Z-axis will pass through the north pole, the Y-axis will pass through the intersection of the equator and prime meridian and the X-axis will pass through  $0^\circ N 90^\circ W$ . The sum of earth's mean radius, local surface altitude (see section on horizon shading) and system pole height is used to translate the array in the X direction.

$$\begin{bmatrix} X_1 \\ Y_1 \\ Z_1 \end{bmatrix} + \begin{bmatrix} 6.371 \times 10^6 + altitude + pole\ height \\ 0 \\ 0 \end{bmatrix} = \begin{bmatrix} X_2 \\ Y_2 \\ Z_2 \end{bmatrix}$$

**Equation 3:** Coordinate translation to Earth center

Finally, the latitude and longitude of each array are applied as rotations to determine the correct earth position and locate the arrays properly relative to one another (see Equation 4). Rotation about the X-axis for latitude followed by rotation about the Z-axis for longitude will achieve the desired effect.

$$\begin{bmatrix} \cos(lon) & -\sin(lon) & 0 \\ \sin(lon) & \cos(lon) & 0 \\ 0 & 0 & 1 \end{bmatrix} \begin{bmatrix} 1 & 0 & 0 \\ 0 & \cos(lat) & -\sin(lat) \\ 0 & \sin(lat) & \cos(lat) \end{bmatrix} \begin{bmatrix} X_2 \\ Y_2 \\ Z_2 \end{bmatrix} = \begin{bmatrix} X_3 \\ Y_3 \\ Z_3 \end{bmatrix}$$

**Equation 4:** Coordinate transformation to arrange arrays on Earth

With arrays oriented and placed correctly relative to one another, we normalize the position relative to an arbitrarily selected reference array to reduce coordinate magnitudes (see Equation 5).

$$\begin{bmatrix} X_{3,array\ N} \\ Y_{3,array\ N} \\ Z_{3,array\ N} \end{bmatrix} - \begin{bmatrix} X_{3,array\ ref} \\ Y_{3,array\ ref} \\ Z_{3,array\ ref} \end{bmatrix} = \begin{bmatrix} X_{4,array\ N} \\ Y_{4,array\ N} \\ Z_{4,array\ N} \end{bmatrix}$$

**Equation 5:** Translation to center coordinates on site

Angular transformations are then performed in reverse order with angular values of opposite sign to move the entire collection of arrays back to a view in which the array normals are parallel to the Z-axis. To maintain correct relative locations during these reverse transformations, the angular values used are those of the reference array. The translation step is skipped during reverse rotations since only relative position of the arrays is important for determining self-shading losses.

Following all transformations, individual module locations can be determined relative to the bottom corner of the array using geometric information about the array layout. The percent shading for each module is calculated using the X, Y, and Z coordinates of array edges to determine which arrays completely or partially obscure the module. The algorithm that performs this calculation is capable of complex shading patterns that could be created when multiple arrays partially shade a module, as illustrated in Figure 2. For shading calculations, the sun is approximated as a point light source due to the significant additional time required during runtime to incorporate penumbral shading effects.

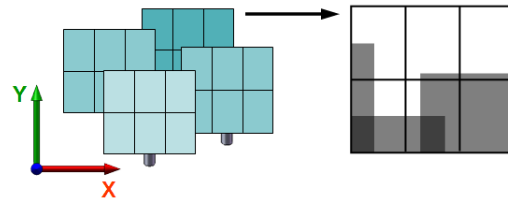


**Figure 2:** Projected view of arrays along ephemeral angle, and representation of resultant partial shading. Darker tone indicates where multiple edges overlap.

## 2.2 Shading model – bulk shading

After self-shading, the other significant source of loss caused by shadows cast on the arrays occurs when the sun is blocked by local or distant obstructions such as buildings, trees, hills and mountains. Since the SolFocus Energy Model was intended to be a flexible tool capable of generating energy forecasts for existing or potential sites, the main focus of efforts to capture bulk shading losses was focused on data that could be easily acquired for any reasonable location in the world. This requirement led to the model making use of the data set available from the Shuttle Radar Tomography Mission (SRTM). This was an international project completed in 2000 using a United States space shuttle that was

specially equipped to map the earth's elevation on a near-global scale [6]. Data sampled at 3 arc second intervals (approximately 90 meters) is publicly available and is downloaded as needed to determine the regional topography [7]. This topography is used to calculate elevations for every tracker and can also be used to generate a horizon profile for any location from 56°S to 60°N.

A horizon profile is generated by calculating angular horizon elevations across the range of compass orientations around the site, typically at 1° intervals. Each calculation consists of an exploration of the topography in the given orientation direction. At regular, small intervals radiating out from the viewer's location, the altitude relative the site is calculated using bilinear interpolation of the SRTM data. Finally, the angular elevation for each point is determined using an equation that includes the curvature of the earth decreasing the apparent height of distant objects. The schematic in Figure 3 is a visual representation of the derivation of this equation.

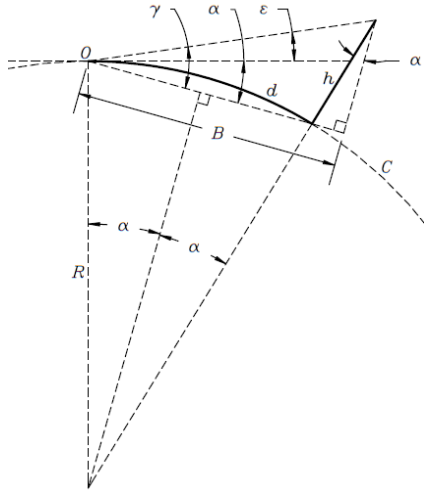


**Figure 3:** Geometric determination of angular subtense of horizon features for bulk shading calculations

$O$  is the viewer's location,  $d$  is the surface distance to the point of interest,  $h$  is the height at the point relative to the origin,  $R$  is the earth's radius at the origin (including altitude above sea level) and  $\epsilon$  is the angular height of the object above the viewer's horizon. The derived equation for this angular height in degrees is shown in Equation 6.

$$\epsilon = \gamma - \alpha = \tan^{-1} \left[ \frac{h}{(2R + h) \tan(\alpha)} \right] - \frac{180d}{C}$$

**Equation 6:** Angular subtense of horizon for a particular azimuth

The maximum perceived height calculated along each bearing is considered to be the angular elevation of the horizon in that direction.

If knowledge of more localized effects is desired (i.e. shading caused by trees and buildings) another means is required for generating the horizon profile since the SRTM data is too coarse to resolve such details. One solution to this problem is to use a device such as the SunEye from Solmetric [8]. This device takes a 180°

image of the whole sky using a fisheye lens and uses image processing techniques to generate a horizon profile which the SolFocus Energy Model can use as input.

In a comparison between the SunEye data and the horizon generated using the SRTM data (see Figure 4), the two were shown to be comparable in shape although the SunEye appeared to truncate information below 5°. Since this approximation has a measurable effect on the model accuracy, SolFocus defaults to using the SRTM data set unless local data is available that captures information about obstacles absent from the shuttle tomography data.

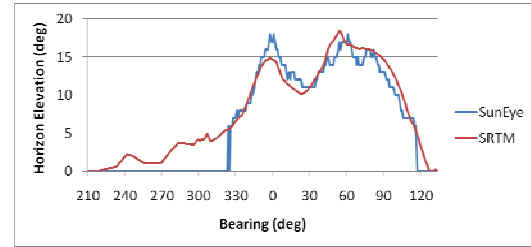


**Figure 4:** Comparison of horizon derived from SRTM data and local imaging obtained from commercial equipment

### 2.3 Electrical connectivity

In general, it is advantageous to construct large tracking assemblies to distribute the cost of tracking hardware over as many modules as possible. These large arrays present some critical design decisions in terms of series and parallel interconnection between solar panels. It is beneficial to combine modules in series with one another to minimize series resistance losses but this is limited by peak voltages allowed under local electrical codes. The typical result of these design constraints is that an array of solar panels is subdivided into multiple series-connected groups; we refer to each of these groups as an electrical string. Strings of modules are connected to a maximum power point tracker (MPPT) which attempts to optimize power output for all strings connected to it. Each MPPT may be connected to one or more strings. In the case of multiple strings, they are connected in parallel (and therefore have the same voltage) at the inverter. To date, most SolFocus plants in operation have one inverter per tracking assembly that services the multiple strings present on that array.

Because of the way modules are connected to one another, under partial shading the power that is produced is highly dependent on the geometric definition of the strings. Figure 5 illustrates two possible scenarios. In these sample cases, each array has 16 modules which are divided up into 4 color-coded strings which are connected in parallel to an MPPT (red dot). The gray rectangle is a shadow cast on the lower right quarter of the array. The MPPT is designed to identify the correct voltage at which the system should operate to produce peak power. As circumstances change incrementally, the peak moves with respect to voltage and the MPPT will follow it. In the example at left, if the illumination situation were to develop gradually, it is possible that the MPPT would follow a peak down to zero volts as produced by a string that is 100% shaded. If this were the case, even though the array is 75% illuminated, it would produce no power. A more intelligent MPPT

would realize that another voltage peak existed which would operate 3 of the 4 strings at 100% while turning off the 4th entirely.

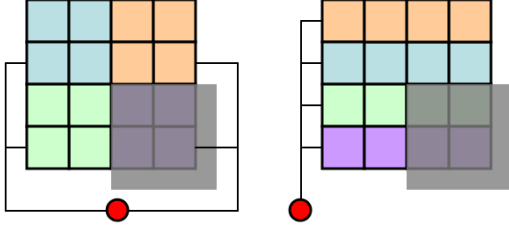


**Figure 5:** Illustrative examples of partial shading on array power with particular electrical interconnection

The example at right will produce only 50% power even with an MPPT that has the ability to find the global peak. Either the two partially shaded strings will be turned off completely allowing the two unshaded to operate at 100% or the two partially shaded strings will operate at 50% pulling down the two remaining strings to 50% as well. These examples illustrate the importance of incorporating time-sensitive string effects into any energy prediction model. The SolFocus Energy Model incorporates an MPPT capable of identifying the global operating peak at all times while discarding solutions outside of a typical MPPT range.

Though the examples above depict an array that is easily divided into rectangular strings of varying shapes, practical considerations can often dictate more complex scenarios. As an illustration (see Figure 6), SolFocus' production system incorporates 4 rows of 7 modules each in the string configuration shown below that minimizes the distance from the string ends to a central point on the array from which they can connect to the inverter. This results in lower wire costs and losses associated with wire resistance. Having a tool capable of analyzing this other non-rectangular or discontinuous string configurations is critical for accurately representing tradeoffs present in a HCPV power system.

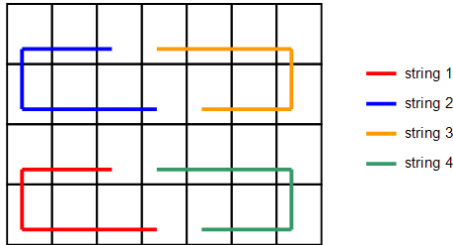


**Figure 6:** Illustration of non-rectangular string areas for SolFocus SF-1100S commercial system.

#### 2.4 Environmental conditions

The environmental model provides a means of estimating instantaneous changes in the maximum power point ( $P_{mp}$ ) given prevailing environmental conditions. This type of environmental dependence has been previously determined by multivariate regression (cite ASTM E-2527-06). For this work, we improve the utility of the environmental model by explicitly including spectral mismatch effects, and by providing derivations of the temperature effects to allow for expedient simulation of updates to the cell and optical design. The

form of the environmental model  $F[t]$  in this work is shown in Equation 7.

$$F[t] = \left\{ 1 + C_T \times (T[t] - T_{Rated}) + C_{DNI} \times (DNI[t] - DNI_{Rated}) + C_{WS} \times (WS[t] - WS_{Rated}) + (SMM[AM] - SMM[AM_{Rated}]) \right\}$$

**Equation 7:** Functional effect of environmental factors on array output power

where

Term	Description	Unit
$T[t]$	Ambient temperature at time t	C
$C_T$	Coefficient of temperature sensitivity	1/C
$T_{Rated}$	Ambient temperature for which rating applies	C
$WS[t]$	Wind speed at time t	m/s
$C_{WS}$	Coefficient of wind speed sensitivity	s/m
$WS_{Rated}$	Wind speed for which rating applies	m/s
$C_{DNI}$	Coefficient of insolation sensitivity	$m^2/W$
$DNI[t]$	DNI at time t	$W/m^2$
$SMM[AM]$	Spectral mismatch due to Rayleigh scatter differing from rating, parameterized by Air Mass	
$AM_{Rated}$	Air Mass that results in reference DNI spectrum	Air Mass

**Table I:** Description of terms used in environmental factors

Note that  $F[t]=1$  when the environmental conditions match the rating conditions.

The optical system transmissivity is taken as constant over the range of module operating conditions; hence, changes in module efficiency arise from changes in operating cell efficiency. The sensitivity of the cell efficiency (mediated by changes in open circuit voltage, or  $V_{OC}$ ) to cell operating temperature is reported on cell manufacturer datasheets [9]. For convenience in matching to tabulated weather data, effects of ambient temperature and heating due to insolation are computed separately. The coefficient of temperature sensitivity is derived as shown in Equation 8.

$$C_T = \frac{d\eta_{rel}}{dT_{amb}} = \frac{1}{\eta_{abs}|_{NOCT}} \times \left( \frac{\partial T_{Cell}}{\partial T_{amb}} \times \frac{\partial \eta_{abs}}{\partial T_{Cell}} \right).$$

**Equation 8:** Derivation of coefficient of temperature sensitivity

For this first order analysis, we take  $\delta T_{Cell}/\delta T_{amb}=1$ .  $1/\eta_{abs}$ , and  $\delta \eta_{abs}/\delta T_{Cell}$  are taken from the cell datasheet for our modules rating conditions. The coefficient of insolation sensitivity is derived as shown in Equation 9.

$$C_{DNI} = \frac{d\eta_{rel}}{dDNI} = \frac{1}{\eta_{abs}|_{NOCT}} \times \left[ \frac{\partial \eta_{abs}}{\partial DNI} + \left( \frac{\partial T_{Cell}}{\partial DNI} \times \frac{\partial \eta_{abs}}{\partial T_{Cell}} \right) \right].$$

**Equation 9:** Derivation of coefficient of insolation sensitivity

At rating conditions, we operate very near the peak of the

concentration vs. efficiency curve; hence, we take  $\delta\eta_{\text{abs}}/\delta\text{DNI}=0$  as a simplifying approximation.

The effect of finite windspeed is to improve the removal of heat from the module, and promote a lower cell operating temperature rise over ambient. The magnitude of the effect depends on wind direction relative to solar angular position, air density, and details on the mounting of modules in creating a system. Given the complexity of interactions, and the typically small effect, we take a conservative stance and approximate  $C_{\text{ws}}=0$ .

The cell operating temperature primarily affects  $V_{\text{OC}}$ . Changes in the spectrum of the DNI insolation affect the efficiency with which solar resource is converted to electrical power. These effects can be determined experimentally for a given optical design in changes to fill factor (FF) and the ratio  $I_{\text{SC}}/\text{DNI}$ . These effects are observed for representative modules, on days of high atmospheric clarity (to best represent typical conditions at sites most suited to HCPV). The product of FF and  $I_{\text{SC}}/\text{DNI}$  is charted against prevailing air mass, and normalized to the air mass rating condition (typically 1.5). Interpolations of these experimentally observed values serve as the SMM[AM] used during simulation of F[t].

### 2.5 Time granularity

The environmental data described in the previous section is available from a number of sources including typical meteorological year (TMY) data [10], and Meteonorm [11]. Data from both of these sources typically is available in one hour intervals. The software can also use field data from a specific site when available. Although values like temperature and DNI change relatively slowly on hourly samples and don't introduce large errors at the TMY data sampling rate, the case is different for shading. Figure 7 illustrates the time dependent nature of partial shading.

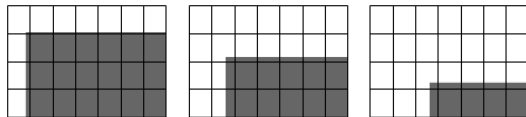


**Figure 7:** Illustration of time dependent partial shading on autumnal equinox in Mountain View, CA of one 7.9m by 5.6m array on a second array 19m to the west, at 6:20 AM, 6:40 AM, and 7AM

The rapid movement of shadows over relatively brief time intervals motivated SolFocus to use a 5 minute sampling rate for shading calculations which, in turn, required interpolation of the available environmental data. Sampling at intervals shorter than 5 minutes was not found to significantly improve accuracy in shading, and encumbers risk of transient temperature responses for the SolFocus panels. Linear interpolation alone was sufficient in the cases of wind speed and temperature but extra information was available for DNI in the form of sunrise and sunset times. This extra knowledge provided a 0-value starting point from which interpolated values could ramp to measured data points. The interpolated curve was scaled so that its integral across the day would be equal to that of the measured points each held for an hour.

In addition to using the finer sampling interval of 5

minutes, the trapezoidal rule is used in the energy summation to improve the approximation of the underlying integral. This approach provides a good alternative to further reduction of the sampling rate which would substantially increase computation time.

### 2.6 Other losses

The other losses category incorporates a wind stow mode as well as bulk losses that can be multiplied by the result during the simulation. The wind stow mode causes the tracker to stop tracking the sun and move to a safe orientation. Bulk losses include AC and DC wire losses, inverter efficiency, soiling, etc.

## 3 MODEL IMPLICATIONS

HCPV plants are scalable from the unit of a single array onward. Self-shading loss is inherently a function of HCPV plant scale, varying from none for an isolated array and converging to some ratio as the plant scale increases without limit. Understanding this effect on energy harvest is important for proper estimation of optimal HCPV plant scale and return on investment. The simulation tool is capable at any scale; however, the  $N^2$  nature of the self-shading leads to diverging run times. A computationally efficient, accurate, method to determine self-shading loss for large plant scales is important.

The self-shading loss is also dependent on the potential energy harvest at low solar elevation. As a thought experiment, for a given plant scale and tracker spacing, sufficiently great horizon shading would result in no solar resource availability for solar elevations relevant to self-shading, and no attributable self-shading loss. Likewise, were adverse environmental conditions to prevail during low solar elevations (e.g., early morning cloudiness, late afternoon high ambient temperatures, high wind speeds at either or both times), self-shading (and horizon shading) impacts are reduced. Hence, the losses due to shading will depend on site climate, and only aggregate losses for all environmental factors, shading, and wind stow are unique. We will term these aggregate losses FSW losses.

Taken together, we anticipate that FSW losses vs. plant scale are a stochastic process in site climate and characteristics. Further, if the relation to plant scale for a given site is sufficiently predictable, we may make computationally efficient, yet accurate extrapolations of FSW losses to very large scales based on a few trials at small plant scales.

In Figure 8 we show the program runtime against the number of trackers in the plant. The computer system was equipped with Windows XP SP3, an Intel Core2 T7400 microprocessor with a 2.16 GHz clock, and 2GB of RAM. The trendline demonstrates a near  $N^2$  dependence in number of trackers as anticipated.

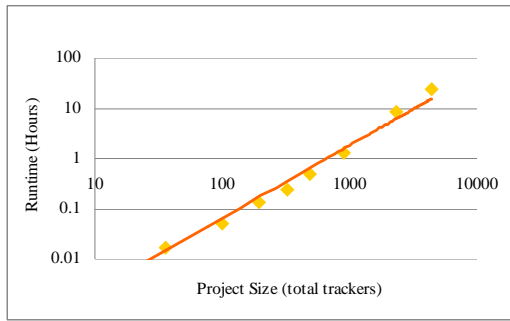


**Figure 8:** Simulation runtime for increasing project scale

In Figure 9 we conduct a study of FSW losses against plant scale for various USA southwest sites of potential interest for HCPV projects. The site climates are obtained from USA TMY data. In each instance, the HCPV plant has arrays placed on a square grid, with North/South columns and East/West rows, and a ratio of array area to tracker spacing of approximately 15%. Each array has a dedicated inverter. The scale of the plant is indicated in terms of the ratio of trackers along one edge of the square grid to the total number of trackers at the plant (e.g., a 4x4 square grid is edge/total=0.25). We use this edge/tracker representation as it has physical appeal regarding the self-shading scaling as edge trackers have different self-shading, and as we have found this mapping effectively linearizes the scaling of self-shading.

As anticipated, there is substantial site to site variation in FSW losses, supporting the need to perform simulation including site characteristics at the plant design stage to assure accurate energy harvest predictions. We also find that self-shading vs. plant scale is predictable, and a linear extrapolation from small plant sizes can provide an accurate estimate of FSW losses at substantially larger plant scales. For example, for the Flagstaff case, a linear extrapolation based on trials of 4x4, 5x5, and 6x6 plant scales can predict FSW losses at the scale of 10x10 to within 0.02%. Further extrapolation to 20x20 plant scale of the same line is accurate only to 0.03%. This result suggests that computational efficiency can be increased more than 10 times for  $N^2$  scaling by extrapolation while retaining a high level of accuracy.

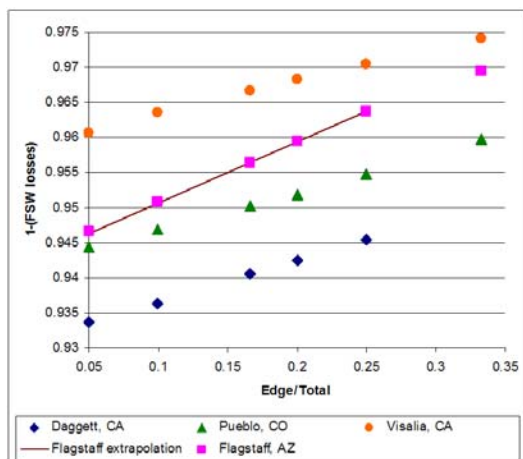


**Figure 9:** Environmental losses for various sites and plant scales

## 4 CONCLUSIONS

We have shown the derivation of a time sequence model for accurate prediction of HCPV plant energy harvest accounting for site weather, site topography, and plant layout. We have shown that shading losses are predictable in plant scale, and that this property allows computationally efficient extrapolation to estimate losses on large plants. With this tool, a site designer can accurately assess site suitability, and optimize tradeoffs in plant layout.

## 5 REFERENCES

- [1] F. Rubio, et al., International Conference on Solar Concentrators 5, (2009).
- [2] Homer simulation tool, [www.homerenergy.com](http://www.homerenergy.com).
- [3] Solar Advisor Model, [www.nrel.gov/analysis/sam](http://www.nrel.gov/analysis/sam).
- [4] PVSYS, [www.pvsyst.com](http://www.pvsyst.com).
- [5] Solar Pro, [www.lapsys.co.jp](http://www.lapsys.co.jp).
- [6] T. Farr, et al., Rev. Geophys., 45, RG2004 (2007).
- [7] [dds.cr.usgs.gov/srtm/version2\\_1/SRTM3](http://dds.cr.usgs.gov/srtm/version2_1/SRTM3).
- [8] [www.solmetric.com](http://www.solmetric.com).
- [9] CDO-100 Concentrator Photovoltaic Cell, [http://www.spectrolab.com/DataSheets/TerCel/C1MJ\\_CDO-100.pdf](http://www.spectrolab.com/DataSheets/TerCel/C1MJ_CDO-100.pdf).
- [10] TMY products available at [apps1.eere.energy.gov/buildings/energyplus/cfm/weather\\_data.cfm](http://apps1.eere.energy.gov/buildings/energyplus/cfm/weather_data.cfm).
- [11] Commercial software available at [www.meteonorm.com](http://www.meteonorm.com).

## 6 ACKNOWLEDGEMENTS

We gratefully acknowledge the support of the SolFocus engineering staff.